XI International Conference on Computational Plasticity. Fundamentals and Applications
COMPLAS XI
E. Oñate, D.R.J. Owen, D. Peric and B. Suárez (Eds)

IMPLEMENTATION OF A MATERIAL MODEL FOR A CAST TRIP-STEEL

Stefan Prüger*, Meinhard Kuna*, Kai Nagel† and Horst Biermann†

*TU Bergakademie Freiberg
Institute for Mechanics and Fluid Dynamics
Lampadiusstrasse 4, 09599 Freiberg, Germany
email: Stefan.Prueger@imfd.tu-freiberg.de

†TU Bergakademie Freiberg
Institute of Materials Engineering
Gustav-Zeuner-Strasse 5, 09599 Freiberg, Germany

Key words: TRIP-steel, finite element implementation, affine trust-region method, notched tensile test

Abstract. The implementation of a phenomenological, macroscopic model for TRIP-steels in the finite element code ABAQUS is presented. The model takes into account both the strain-rate dependent flow behaviour of the two phases, austenite (γ) and martensite (α'), and the temperature and stress state dependent $\gamma \rightarrow \alpha'$ phase transformation. In order to solve the system of nonlinear equations, which results from the implicit integration of the constitutive model, the application of an affine trust-region approach is proposed to compute strictly feasible solutions. Furthermore, model predictions are compared with experimental results obtained from tensile tests on notched specimens.

1 INTRODUCTION

A common feature of many TRIP-steels is their favourable combination of high strength and pronounced ductility. These properties also apply to a newly developed as cast TRIP-steel [1] and are attributed to the inelastic deformation of the two phases austenite (γ) and martensite (α') and the strain-induced $\gamma \rightarrow \alpha'$ phase transformation, which accompanies the deformation. The cast TRIP-steel possesses a fully austenitic, coarse grain initial microstructure and the transformation proceeds by the formation of shear bands within the grains and subsequent nucleation of martensite within these bands [2]. It has been found that the transformation behaviour is rather sensitive to temperature and strain rate [3]. Therefore, an adequate material model is required to describe the complex material behaviour of the TRIP-steel.
An approach, which has been successfully applied to develop macroscopic models for

TRIP-steels relies on the computation of effective properties of composites. Herein, TRIP-steels are considered as composites with evolving microstructure [4], [5], [6]. In the current paper, we also follow this approach and give an extension of the model proposed in [6]. The composite approach is advantageous, because it allows insight into the stress and strain levels in the single phases of the TRIP-steel as their constitutive response is explicitly taken into account. However, the burden of such a procedure is the increased complexity and possibly additional nonlinearity of the model due to the required homogenisation process. Therefore, more elaborated numerical methods might be required to solve the nonlinear equations, associated with the implicit integration of the constitutive model. Besides the required starting point, the physical nature of the independent variables or numerical considerations impose certain restrictions on these variables in order to exclude infeasible solutions. In case of viscoplastic models, it has been shown by de Souza Neto [7] that the commonly applied Newton's method is not appropriate to handle such bounds. In this paper an affine trust-region method [8] is applied to solve the bound constrained nonlinear equations, which arise from the implicit integration procedure.
Throughout this paper symbolic notation is employed, where $\mathbb{A}$ and $\mathbf{A}$ denote fourth order and second order tensors, respectively. The norm of $\mathbf{A}$ is defined as $\|\mathbf{A}\| = \sqrt{\mathbf{A} : \mathbf{A}}$. Vectors are given in matrix notation, i.e. the norm of a vector is described as $\|\mathrm{A}\| = \sqrt{\mathrm{A}^{\mathrm{T}}\mathrm{A}}$. The Jacobian of a vector function $\mathrm{F(x)}$ is introduced as $\mathrm{F}' = \frac{\partial F_i}{\partial x_j}$. The fourth order isotropic tensor and the Kronecker symbol are given as $\mathbb{I} = \frac{1}{2}(\delta_{ik}\delta_{jl} + \delta_{il}\delta_{jk})e_i \otimes e_j \otimes e_k \otimes e_l$ and $\mathbf{I} = \delta_{ij}e_i \otimes e_j$, respectively. The material time derivative is expressed as $\dot{(\ )} = \frac{\mathrm{d}(\ )}{\mathrm{d}t}$.

2 MATERIAL MODEL

In order to describe the response of the TRIP-steel under arbitrary large deformations, the finite deformation theory is employed to formulate the corresponding constitutive equations. An additive split of the rate of deformation tensor according to

$$\mathbf{D} = \mathbf{D}^{\mathrm{e}} + \mathbf{D}^{\mathrm{vp}} + \mathbf{D}^{\mathrm{trip}} \tag{1}$$

is carried out. The elastic and the viscoplastic rates of deformation are denoted by $\mathbf{D}^{\mathrm{e}}$ and $\mathbf{D}^{\mathrm{vp}}$, respectively, whereas the rate of deformation associated with the phase transformation is termed $\mathbf{D}^{\mathrm{trip}}$. The assumption of small elastic strains, generally valid in metal plasticity, allows to formulate the constitutive law as a linear, hypoelastic relation

$$\overset{\triangledown}{\mathbf{\Sigma}} = \mathbb{C} : \mathbf{D}^{\mathrm{e}} \tag{2}$$

that connects the Jaumann rate of the Cauchy stress and the elastic rate of deformation tensor [9]. In the case of isotropic elasticity the elastic modulus tensor

$$\mathbb{C} = 2G\mathbb{I} + (K - \frac{2}{3}G)\mathbf{I} \otimes \mathbf{I} \tag{3}$$

is described in terms of the shear modulus G and the bulk modulus K. This approach assumes identical elastic properties of the two phases austenite and martensite. The viscoplastic rate of deformation is defined as

$$\mathbf{D}^{\mathrm{vp}} = \frac{1}{2}\Theta^{\mathrm{hom}}\mathbf{S}, \tag{4}$$

where $\mathbf{S}$ denotes the deviator of the Cauchy stress and Θ^{hom} the viscoplastic compliance of the two-phase composite, which is determined by homogenising the viscoplastic response of the single phases. During phase transformation both volumetric and deviatoric deformations occur. Therefore, the rate of deformation associated with the phase transformation takes the form

$$\mathbf{D}^{\mathrm{trip}} = \dot{f}_m \left(R\mathbf{N} + \frac{1}{3}\Delta_v \mathbf{I} \right) \ . \tag{5}$$

Herein, the volumetric transformation strain is denoted by Δ_v, while

$$R = R_0 + R_1 \frac{\bar{\Sigma}}{\sigma_a^*} \tag{6}$$

is the stress dependent magnitude of the deviatoric transformation strain, whose direction is given in terms of the normalized stress deviator $\mathbf{N} = \mathbf{S}/\|\mathbf{S}\|$. The von Mises equivalent stress is computed as $\bar{\Sigma} = \sqrt{\frac{3}{2}}\|\mathbf{S}\|$. The transformation strain is controlled by the rate of the martensite volume fraction $\dot{f}_m$.

Due to the significant difference in the flow behaviour of the two phases, their rate dependent flow behaviour is modeled separately. Therefore, each phase is described by a unified viscoplastic model of the von Mises type, i.e. the viscoplastic deformation is strictly deviatoric. The viscoplastic equivalent strain rate is defined as

$$\dot{\bar{\varepsilon}}^{\mathrm{vp}}_{(r)} = \dot{\varepsilon}^{0}_{(r)} \left(\frac{\tilde{\sigma}_{(r)}}{\sigma^{\mathrm{y}}_{(r)}} \right)^{m_{(r)}} \ , \tag{7}$$

where $\tilde{\sigma}_{(r)}$, $\sigma^{\mathrm{y}}_{(r)}$ and $\dot{\varepsilon}^{0}_{(r)}$ denote the equivalent stress, the yield stress and the reference strain rate of the phase r, which can be either austenite (a) or martensite (m). The isotropic strain hardening of each phase is considered by using the power law

$$\sigma^{\mathrm{y}}_{(r)} = A_{(r)} + B_{(r)} (\bar{\varepsilon}^{\mathrm{vp}}_{(r)})^{q_{(r)}} \ . \tag{8}$$

According to the variational principle for the homogenisation of nonlinear composites, described in [10], the equivalent stresses $\tilde{\sigma}_{(r)}$ can be related to macroscopic equivalent stress $\bar{\Sigma}$ as

$$\tilde{\sigma}_{(r)} = \bar{\Sigma} \sqrt{\frac{1}{f_{(r)}} \frac{\partial \Theta^{\mathrm{hom}}}{\partial \Theta_{(r)}}} \ . \tag{9}$$

This relation holds, if the composite consists of isotropic phases arranged in a statistically uniform and isotropic manner. In order to evaluate this expression, a description of the homogenised compliance Θ^{hom} in terms of the compliances of the single phases $\Theta_{(r)}$ is required. Here the bound

$$\Theta^{\mathrm{hom}} = \frac{f_m(\frac{2}{\Theta_a} + \frac{3}{\Theta}) + f_a(\frac{2}{\Theta_m} + \frac{3}{\Theta})}{\frac{f_m}{\Theta_m}(\frac{2}{\Theta_a} + \frac{3}{\Theta}) + \frac{f_a}{\Theta_a}(\frac{2}{\Theta_m} + \frac{3}{\Theta})} \,, \tag{10}$$

as proposed by Hashin Shtrikman [11], is used. It should be noted that $\Theta = \max(\Theta_a, \Theta_m)$ and the volume fraction of austenite is defined as $f_a = 1 - f_m$. The viscoplastic compliances of the single phases

$$\Theta_{(r)} = \frac{3}{\tilde{\sigma}_{(r)}} \dot{\bar{\varepsilon}}^{\mathrm{vp}}_{(r)} = \frac{3\dot{\varepsilon}^0_{(r)}}{\tilde{\sigma}_{(r)}} \left(\frac{\tilde{\sigma}_{(r)}}{\sigma^{\mathrm{y}}_{(r)}} \right)^{m_{(r)}} \tag{11}$$

correspond to a linearized form of Eq. (7).
In order to describe the phase transformation behaviour of the cast TRIP-steel, the macroscopic transformation model by Stringfellow [5] is extended. This model is inspired by the experimental observation that martensite nucleates predominantly at shear band intersection, which have been formed prior to the nucleation event. Following the derivation in [5], an evolution equation for the martensite volume fraction of the form

$$\dot{f}_m = (1 - f_m)(A\dot{\bar{\varepsilon}}^{\mathrm{vp}}_a + B(\dot{g} - \dot{\bar{g}})) \tag{12}$$

is proposed. Herein, the thermodynamical driving force g for the martensite evolution

$$g = g_0 - g_1\vartheta + g_2\vartheta^2 + g_3(\Delta_v p + \sqrt{\frac{2}{3}} R\bar{\Sigma}) \tag{13}$$

is taken as a function of the hydrostatic stress $p = \frac{1}{3}\boldsymbol{\Sigma} : \mathbf{I}$, the von Mises equivalent stress $\bar{\Sigma}$ and the normalized temperature ϑ

$$\vartheta = \frac{T - M^\sigma_{\mathrm{s}}}{M_{\mathrm{d}} - M^\sigma_{\mathrm{s}}}, \tag{14}$$

where T and M^σ_{s} correspond to the temperature and the start temperature for stress-induced martensite formation, respectively. M_{d} is the highest temperature, at which martensite can be mechanically induced [12]. The mean transformation barrier $\bar{g}$ is assumed to depend on the viscoplastic equivalent strain in the austenite in the form

$$\bar{g} = \bar{g}_0 + \bar{g}_1 \bar{\varepsilon}^{\mathrm{vp}}_a \,. \tag{15}$$

This approach incorporates the effect that the energy required for the accommodation of the martensite nuclei in the surrounding matrix material depends on the viscoplastic

deformation of the austenite prior to the nucleation [13]. The parameter A that controls the martensite formation due to an increase in nucleation sites is given as

$$A = a\beta n (f_{SB})^{n-1}(1 - f_{SB})P \ . \tag{16}$$

The formation of shear bands in austenite is modeled via the volume fraction of shear bands f_{SB}, whose evolution is described according to

$$\dot{f}_{SB} = (1 - f_{SB})a\dot{\bar{\varepsilon}}_a^{\mathrm{vp}} \ . \tag{17}$$

The rate of shear band formation a is taken as function of the temperature T and the stress triaxiality $h = p/\bar{\Sigma}$ in the form

$$a = a_1 + a_2 T + a_3 T^2 - a_4 \arctan(h) \ . \tag{18}$$

To account for the observation that under given values of the driving force and the transformation barrier martensite is formed only at a certain fraction of potential nucleation sites, the following function P is introduced.

$$P = \frac{1}{\sqrt{2\pi} s_g} \int_{-\infty}^{g} \exp\left[-\frac{1}{2}\left(\frac{g' - \bar{g}}{s_g}\right)^2\right] \mathrm{d}g' \tag{19}$$

The parameter B, which incorporates the change in martensite volume fraction due to a change in the driving force and the transformation barrier is given as

$$B = \beta (f_{SB})^n \frac{\mathrm{d}P}{\mathrm{d}g} H(\dot{P}) \ . \tag{20}$$

It should be noted that β, n and $H(\dot{P})$ in equation (16) and (20) describe two geometrical constants and the unit step function, respectively.

3 IMPLEMENTATION

3.1 Integration of the material model

The constitutive model, described in Sect. 2, is implemented in the finite element program ABAQUS using the user subroutine interface UMAT. The applied incremental, iterative solution strategy requires the integration of the rate form of the constitutive equations in the context of finite deformations over a finite time increment $\Delta t = t|_{n+1} - t|_n$. In the following, quantities at the beginning and the end of the increment are indicated by $()|_n$ and $()|_{n+1}$, respectively, while the increments of these quantities are defined as $\Delta = ()|_{n+1} - ()|_n$. The integration is carried using the algorithm proposed by Hughes and Winget [14], because it preserves the objectivity incrementally. When applied to a second order tensor $\mathbf{A}$, it takes the form

$$\mathbf{A}|_{n+1} = \Delta\mathbf{R} \cdot \mathbf{A}|_n \cdot \Delta\mathbf{R}^{\mathbf{T}} + \Delta\mathbf{A}(\Delta\mathbf{E}), \tag{21}$$

where $\Delta\mathbf{R}$ and $\Delta\mathbf{E}$ denote the increment in rotation and an approximation of the strain increment, respectively. The last term of the right hand side corresponds to the change in $\mathbf{A}$ as a result of the strain increment $\Delta\mathbf{E}$ associated with Δt. Under suitable assumptions regarding the rotation of the principle axis of the strain, the time integration of Eq. (1) yields the incremental relation

$$\Delta\mathbf{E} = \Delta\mathbf{E}^{\mathrm{e}} + \Delta\mathbf{E}^{\mathrm{vp}} + \Delta\mathbf{E}^{\mathrm{trip}}. \tag{22}$$

Due to its unconditional stability, the integration is carried out using a one-step implicit integration scheme. Therefore, the inelastic strain increments are calculated by

$$\Delta\mathbf{E}^{\mathrm{vp}} = \frac{\Delta t}{2}\Theta^{\mathrm{hom}}|_{n+1}\mathbf{S}|_{n+1} \tag{23}$$

and

$$\Delta\mathbf{E}^{\mathrm{trip}} = \Delta f_m \left(R|_{n+1}\mathbf{N}|_{n+1} + \frac{1}{3}\Delta_v\mathbf{I} \right) \ . \tag{24}$$

The stress increment is computed according to

$$\Delta\boldsymbol{\Sigma} = \mathbb{C} : (\Delta\mathbf{E} - \Delta\mathbf{E}^{\mathrm{vp}} - \Delta\mathbf{E}^{\mathrm{trip}}) \tag{25}$$

after the stress at the beginning of the increment is rotated as described in Eq. (21). The constitutive description of the viscoplastic behaviour of the single phases, which has been introduced in Eq. (7),(8) and (11), is given in the discretized form as

$$\dot{\bar{\varepsilon}}^{\mathrm{vp}}_{(r)}|_{n+1} = \dot{\varepsilon}^{0}_{(r)} \left(\frac{\tilde{\sigma}_{(r)}|_{n+1}}{\sigma^{\mathrm{y}}_{(r)}|_{n+1}} \right)^{m_{(r)}} \tag{26}$$

$$\Theta_{(r)}|_{n+1} = \frac{3\dot{\varepsilon}^{0}_{(r)}}{\tilde{\sigma}_{(r)}|_{n+1}} \left(\frac{\tilde{\sigma}_{(r)}|_{n+1}}{\sigma^{\mathrm{y}}_{(r)}|_{n+1}} \right)^{m_{(r)}} \tag{27}$$

$$\sigma^{\mathrm{y}}_{(r)}|_{n+1} = A_{(r)} + B_{(r)}(\bar{\varepsilon}^{\mathrm{vp}}_{(r)}|_{n} + \dot{\bar{\varepsilon}}^{\mathrm{vp}}_{(r)}|_{n+1}\Delta t)^{q_{(r)}} \ , \tag{28}$$

while the equivalent stresses are computed as

$$\tilde{\sigma}_{(r)}|_{n+1} = \bar{\Sigma}|_{n+1}\sqrt{\frac{1}{f_{(r)}|_{n+1}}\frac{\partial\Theta^{\mathrm{hom}}}{\partial\Theta_{(r)}}\bigg|_{n+1}} \ . \tag{29}$$

The evolution of the martensite volume fraction over the time increment Δt is approximated with

$$\Delta f_m = (1 - f_m|_{n+1})(A|_{n+1}\dot{\bar{\varepsilon}}^{\mathrm{vp}}_{a}|_{n+1} + B|_{n+1}(\dot{g}|_{n+1} - \dot{\bar{g}}|_{n+1}))\Delta t \ . \tag{30}$$

The incremental change in the volume fraction of shear bands is obtained from

$$\Delta f_{SB} = (1 - f_{SB}|_{n+1}) a|_{n+1} \dot{\bar{\varepsilon}}_a^{\mathrm{vp}}|_{n+1} \Delta t \ . \tag{31}$$

Using Eq. (13) and (15) the rate of the driving force and the transformation barrier are given at the end of the increment as

$$\dot{g}|_{n+1} = -g_1 \dot{\vartheta}|_{n+1} + 2 g_2 \vartheta|_{n+1} \dot{\vartheta}|_{n+1} + g_3 \left(\Delta_v \dot{p}|_{n+1} + \sqrt{\frac{2}{3}} \left(R + \bar{\Sigma} \frac{\partial R}{\partial \bar{\Sigma}} \right) \Big|_{n+1} \dot{\bar{\Sigma}}|_{n+1} \right) \tag{32}$$

$$\dot{\bar{g}}|_{n+1} = \bar{g}_1 \dot{\bar{\varepsilon}}_a^{\mathrm{vp}}|_{n+1} \ , \tag{33}$$

respectively.
According to Papatriantafillou [6], the nonlinear, implicit tensor equation (25) can be efficiently solved by applying the integration algorithm proposed by Aravas [15] in the case of pressure dependent plasticity models. We follow this approach and state the resulting two nonlinear equation for the stress invariants.

$$p|_{n+1} = p^{\mathrm{trial}}|_{n+1} - K \Delta E^{\mathrm{in}} \tag{34}$$

$$\bar{\Sigma}|_{n+1} = \bar{\Sigma}^{\mathrm{trial}}|_{n+1} - 3G \Delta \bar{G}^{\mathrm{in}} \tag{35}$$

The trial stress $\boldsymbol{\Sigma}^{\mathrm{trial}}$ is obtained from Eq. (25) by

$$\boldsymbol{\Sigma}^{\mathrm{trial}}|_{n+1} = \boldsymbol{\Sigma}|_n + \mathbb{C} : \Delta \mathbf{E} \ . \tag{36}$$

The quantities ΔE^{in} and $\Delta \bar{G}^{\mathrm{in}}$ are defined as

$$\Delta E^{\mathrm{in}} = (\Delta \mathbf{E}^{\mathrm{vp}} + \Delta \mathbf{E}^{\mathrm{trip}}) : \mathbf{I} = \Delta_v \Delta f_m \tag{37}$$

$$\begin{aligned} \Delta \bar{G}^{\mathrm{in}} &= \sqrt{\frac{2}{3} \left(\Delta \mathbf{E}^{\mathrm{vp}} + \Delta \mathbf{E}^{\mathrm{trip}} - \frac{1}{3} \mathbf{I} \Delta E^{\mathrm{in}} \right) : \left(\Delta \mathbf{E}^{\mathrm{vp}} + \Delta \mathbf{E}^{\mathrm{trip}} - \frac{1}{3} \mathbf{I} \Delta E^{\mathrm{in}} \right)} \\ &= \Delta f_m \sqrt{\frac{2}{3}} R|_{n+1} + \frac{\Delta t}{3} \Theta^{\mathrm{hom}}|_{n+1} \bar{\Sigma}|_{n+1} \ . \end{aligned} \tag{38}$$

In order to compute the stress at the end of the increment, $\Delta \bar{G}^{\mathrm{in}}$ and $f_m|_{n+1}$ are taken as the primary unknowns and the Eq. (30) and (38) are reformulated as residuals.
The determination of the quantities at level of the single phases, namely $\dot{\bar{\varepsilon}}^{\mathrm{vp}}_{(r)}|_{n+1}$, $\Theta_{(r)}|_{n+1}$, $\sigma^{\mathrm{y}}_{(r)}|_{n+1}$ and $\tilde{\sigma}_{(r)}|_{n+1}$ requires the solution of the system of equations defined by (26) to (29). According to the proposal in [6], the introduction of the ratio of the viscoplastic compliance $X_m = \frac{\Theta_m}{\Theta_a}$ allows for a reduction of the two nonlinear equations (27) to a single equation. In contrast to [6] the yield stresses in both phases are evaluated at the end of

the increment. Therefore, equation (26) and (29) are included in (28), which leads to the following system of equations

$$X_m|_{n+1} = \frac{\dot{\varepsilon}_m^0}{\dot{\varepsilon}_a^0} \frac{(\sigma_a^{\mathrm{y}}|_{n+1})^{m_a}}{(\sigma_m^{\mathrm{y}}|_{n+1})^{m_m}} \frac{\left(\sqrt{\frac{1}{f_m|_{n+1}} \frac{\partial \Theta^{\mathrm{hom}}}{\partial \Theta_m}\Big|_{n+1}}\right)^{m_m-1}}{\left(\sqrt{\frac{1}{f_a|_{n+1}} \frac{\partial \Theta^{\mathrm{hom}}}{\partial \Theta_a}\Big|_{n+1}}\right)^{m_a-1}} (\bar{\Sigma}|_{n+1})^{m_m-m_a} \tag{39}$$

$$\sigma_a^{\mathrm{y}}|_{n+1} = A_a + B_a \left(\bar{\varepsilon}_a^{\mathrm{vp}}|_n + \Delta t \dot{\varepsilon}_a^0 \left(\frac{\bar{\Sigma}|_{n+1} \sqrt{\frac{1}{f_a|_{n+1}} \frac{\partial \Theta^{\mathrm{hom}}}{\partial \Theta_a}\Big|_{n+1}}}{\sigma_a^{\mathrm{y}}|_{n+1}} \right)^{m_a} \right)^{q_a} \tag{40}$$

$$\sigma_m^{\mathrm{y}}|_{n+1} = A_m + B_m \left(\bar{\varepsilon}_m^{\mathrm{vp}}|_n + \Delta t \dot{\varepsilon}_m^0 \left(\frac{\bar{\Sigma}|_{n+1} \sqrt{\frac{1}{f_m|_{n+1}} \frac{\partial \Theta^{\mathrm{hom}}}{\partial \Theta_m}\Big|_{n+1}}}{\sigma_m^{\mathrm{y}}|_{n+1}} \right)^{m_m} \right)^{q_m} . \tag{41}$$

Note that the derivatives $\frac{\partial \Theta^{\mathrm{hom}}}{\partial \Theta_a}$ and $\frac{\partial \Theta^{\mathrm{hom}}}{\partial \Theta_m}$ also dependent on X_m and the solution of the system of implicit equations requires iterative methods, which are described in Sect. 3.2. Once the above equations are solved together with Eq. (30) and (38), the viscoplastic and the transformation strain can be updated based on the trial stress and determined quantities according to Eq. (23) and (24).
The use of an implicit integration scheme for the constitutive equations necessitates the computation of the consistent material tangent, which is defined as

$$\mathbb{C}^{\mathrm{t}}|_{n+1} = \left.\frac{\partial \boldsymbol{\Sigma}}{\partial \mathbf{E}}\right|_{n+1} = \mathbb{C} - \mathbb{C} : \mathbb{M}|_{n+1} : \mathbb{C} \, . \tag{42}$$

The tensor $\mathbb{M}|_{n+1}$ takes the form

$$\mathbb{M}|_{n+1} = \frac{1}{3} \Delta_v \left.\frac{\partial f_m}{\partial \boldsymbol{\Sigma}^{\mathrm{trial}}}\right|_{n+1} \otimes \mathbf{I} + \frac{3}{2} \left(\left.\frac{\partial \Delta \bar{G}^{\mathrm{in}}}{\partial \boldsymbol{\Sigma}^{\mathrm{trial}}}\right|_{n+1} \otimes \mathbf{M}|_{n+1} + \Delta \bar{G}^{\mathrm{in}} \left.\frac{\partial \mathbf{M}}{\partial \boldsymbol{\Sigma}^{\mathrm{trial}}}\right|_{n+1} \right) . \tag{43}$$

The derivatives of f_m and $\Delta \bar{G}^{\mathrm{in}}$ with respect to the trial stress tensor are obtained by implicit differentiation of the residual form of Eq. (30) and (38). The differentiation of the normalized stress deviator $\mathbf{M} = \mathbf{S}/\bar{\Sigma}$ is carried out consistent with [16]. Note that the resulting consistent material tangent is unsymmetric due to the mutual coupling between f_m and $\Delta \bar{G}^{\mathrm{in}}$.

3.2 Numerical solution of the nonlinear systems of equations

As mentioned in Sect. 3.1, iterative methods are required the solve the two systems of equations $(\mathrm{r_I}, \mathrm{r_{II}})$, which are given by Eqs. (39) to (41) and Eq. (30) and (38), respectively. Due to the choice of independent variables in the corresponding systems, the staggered

solution procedure shown in Fig. 1 is proposed. In order to avoid iterates that are unphysical due to the irreversible nature of the inelastic processes and may lead to numerical difficulties, the following bounds are introduced (see Tab. 1).

Table 1: Bounds on variables

$0 \leq \Delta\bar{G}^{\text{in}}$	$f_m\|_n \leq f_m\|_{n+1}$
$0 \leq X_m\|_{n+1}$	$\sigma_a^{\text{y}}\|_n \leq \sigma_a^{\text{y}}\|_{n+1}$
$\sigma_m^{\text{y}}\|_n \leq \sigma_m^{\text{y}}\|_{n+1}$	

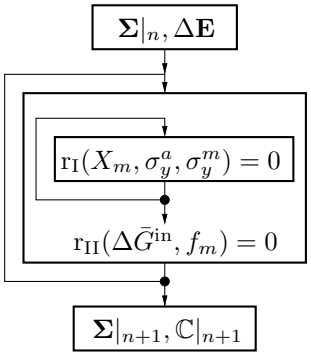

Figure 1: Staggered solution algorithm

As Newton's method is not intended for handling such bounds and truncating the Newton step may result in poor convergence when approaching a bound, an interior global method proposed by Bellavia et al. [8] is used. This method belongs to the group of affine trust-region methods and is able to solve problems of the kind

$$\mathrm{F(x)} = 0 \ , \quad \mathrm{l} \leq \mathrm{x} \leq \mathrm{u} \ , \tag{44}$$

where F is a system of nonlinear equations and x is the vector of independent variables, while l and u denote given lower and upper bounds. As the use of such a method is not commonly employed in the context of constitutive modelling, the method is briefly described. When applying this method to solve Eq. (44), the computed steps are guaranteed to sufficiently reduce the norm $\|\mathrm{F(x)}\|$ and to stay strictly inside the feasible region. This requires the solution of an elliptical trust-region problem

$$\min_{\mathrm{q}} \{ m_k(\mathrm{q}) : \|\mathrm{D}_k \mathrm{q}\| \leq \Delta_k \} \tag{45}$$

at every iteration k, where

$$m_k(\mathrm{q}) = \frac{1}{2}\|\mathrm{F}_k\| + \mathrm{F}_k^{\mathrm{T}}\mathrm{F}'_k\mathrm{q} + \frac{1}{2}\mathrm{q}^{\mathrm{T}}\mathrm{F}'^{\mathrm{T}}_k\mathrm{F}'_k\mathrm{q} \ . \tag{46}$$

The sufficient reduction is ensured by adjusting the step size of q via the trust-region radius Δ_k, while the scaling matrix D_k, which measures the distance of the current iterate to the bound, is used to adapt the current step q in order to generate feasible iterates. According to [8] the method shows quadratic convergence even to solutions on the boundary of the feasible region and is not much more computational expensive than a conventional Newton iteration. Due to these favourable properties, the affine trust-region method is employed in the solution of both systems of equations ($\mathrm{r_I}, \mathrm{r_{II}}$) that arise from the implicit integration of the material model. The interested reader is referred to [8] for convergence proofs and implementation issues.

Table 2: Material parameters

A_a [MPa]	B_a [MPa]	q_a	A_m [MPa]	B_m [MPa]	q_m	a_1	a_4
180	1564	0.83	1429	276	0.86	4.61	0.13
$\bar{g}_0$ $[\frac{mJ}{mm^3}]$	$\bar{g}_1$ $[\frac{mJ}{mm^3}]$	s_g $[\frac{mJ}{mm^3}]$	R_0	R_1	n	β	Δ_v
207	20	178	0.0284	0.0574	2.61	1.4	0.04
M_{s}^{σ} $[°C]$	M_{d} $[°C]$	K [MPa]	G [MPa]	g_0 $[\frac{mJ}{mm^3}]$	g_1 $[\frac{mJ}{mm^3}]$	g_2 $[\frac{mJ}{mm^3}]$	g_3
20	100	123077	77419	330	71.6	0.56	1
σ_a^*	m_a	$\dot{\varepsilon}_a^0$ $[s^{-1}]$	m_m	$\dot{\varepsilon}_a^0$ $[s^{-1}]$	a_2	a_3	
387	30	0.001	40	0.001	0	0	

4 RESULTS

The material model presented in Sect. 2 is applied to describe the deformation behaviour of a newly developed CrMnNi cast TRIP-steel [1]. The model has been calibrated using data from both tensile and compression tests to account for the tension-compression asymmetry included in the model. The mechanical tests were carried out at room temperature under quasistatic loading conditions. Details of the employed parameter identification strategy are given in [17]. The identified parameters are included in the upper half of Tab. 2. Furthermore, the constant parameters listed in the lower half of Tab. 2 are used, which were obtained either by thermodynamical calculation (g_0, g_1, g_2), direct measurement (K, G) or have been assumed as in case of temperature and strain rate dependent material behaviour. In order to evaluate the capabilities of the calibrated model to predict the deformation behaviour under different inhomogeneous triaxial stress states, a series of notched tensile tests has been conducted. The corresponding specimens were manufactured with notch radii $R = \{1, 2, 4, 8\text{mm}\}$. The measurements were accomplished under displacement control at a constant rate of 0.5mm/min employing a servohydraulic test machine MTS Landmark 100. During the test, force and displacement were recorded utilizing the built-in load cell of the test machine and a MTS extensiometer. Additionally, the notch radius and the diameter reduction at the notch root were measured during deformation by an optical extensiometer. Consistent with the experiment, a gauge length $L = 35\text{mm}$, an outer diameter $D = 12\text{mm}$ and a diameter $d = 6\text{mm}$ of the minimum section of the notched tensile specimen were used in the finite element model to simulate the notched tensile tests with the finite element code ABAQUS. Due to the symmetries intrinsic to the problem, only the upper half of the specimen is modeled, employing linear axisymmetrical elements (CAX4). The boundary value problem is depicted in Fig. 2. The displacement in positive z-direction is uniformly prescribed at the top of the specimen according to the experimental procedure. The experimentally determined force displacement curves for different notch radii are shown in Fig. 3 together with the corresponding

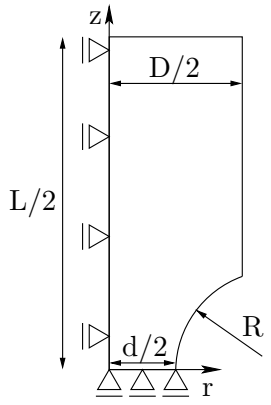

Figure 2: Notched tensile specimen

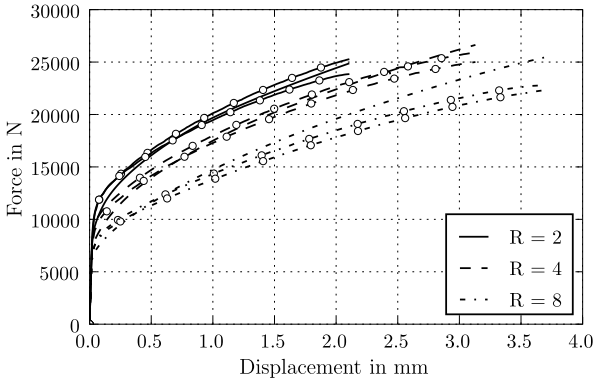

Figure 3: Comparison between experiments (○) and simulation

results of the simulation. Reasonable good agreement between the results from the simulation and the experimental measurements is observed, although the model overestimates the force displacement curve in case of low stress triaxialities. It can be concluded that the model is able to capture the effect of stress triaxiality on the force displacement curve.

5 CONCLUSIONS

In the current paper the implementation of a macroscopic material model for TRIP-steels into the finite element code ABAQUS has been presented. A staggered solution procedure is used to solve the coupled systems of nonlinear equations, which result from the implicit integration of the constitutive model. The computation of infeasible solutions is avoided by applying an affine trust-region approach. The calibrated model is employed to predict the force displacement curve of notched tensile tests. Reasonable good agreement can be observed, if model predictions are compared to experimental results.

ACKNOWLEDGEMENTS

The authors gratefully acknowledge the Deutsche Forschungsgemeinschaft (DFG) for supporting this work carried out in the framework of the Collaborative Research Center TRIP-Matrix composites (SFB 799, C5 and B4).

REFERENCES

[1] Jahn, A. et al., Mechanical properties of high alloyed cast and rolled CrMnNi TRIP steels with varying Ni contents. 05013 (2009), DOI: 10.1051/esomat/200905013.

[2] Martin, S. et al., Investigations on martensite formation in CrMnNi-TRIP steels. 05022 (2009), DOI: 10.1051/esomat/200905022.

[3] Krüger, L. et al., Strain rate and temperature effects on stress-strain behaviour of cast high alloyed CrMnNi-steel. *DYMAT 2009* (2009) 1069-1074 DOI: 10.1051/dy-

mat/2009149.

[4] Cherkaoui, M et al., A phenomenological dislocation theory for martensitic transformation in ductile materials: From micro- to macroscopic description. *Philosophical Magazine* (2008) **88**:3479–3512.

[5] Stringfellow, R. G. et al., A Constitutive Model For Transformation Plasticity Accompanying Strain-Induced Martensitic Transformations In Metastable Austenitic Steels. *Acta Metall. Mater.* (1992) **40**:1703–1716.

[6] Papatriantafillou, I. et al., Constitutive modeling and finite element methods for TRIP steels. *Comput. Method Appl. M.* (2006) **195**:5094–5114.

[7] de Souza Neto, E. A., A simple robust numerical integration algorithm for a power-law visco-plastic model under both high and low rate-sensitivity. *Commun. Numer. Meth. En.* (2004) **20**:1–17.

[8] Bellavia, S. and Morini, B., An interior global method for nonlinear systems with simple bounds. *Optim. Method Softw.* (2005) **20**:453–474.

[9] Needleman, A., On Finite-Element Formulations For Large Elastic Plastic-Deformations. *Comput. Struct.* (1985) **20**:247–257.

[10] Ponte Castañeda, P. and Suquet, P., Nonlinear Composites. *Adv. Appl. Mech.* (1998) **34**:172–302.

[11] Hashin, Z. and Shtrikman, S., Note on a variational approach to the theory of composite elastic materials. *J. Franklin I.* (1961) **271**:336–341.

[12] Olson, G. B. and Cohen, M., Mechanism For Strain-Induced Nucleation Of Martensitic Transformations. *J. Less-Common Met.* (1972) **28**:107–118

[13] Lani, F. et al., Multiscale mechanics of TRIP-assisted multiphase steels: II. Micromechanical modelling. *Acta Mater.* (2007) **55**:3695–3705.

[14] Hughes, T. J. R. and Winget, J., Finite Rotation Effects In Numerical-Integration Of Rate Constitutive-Equations Arising In Large-Deformation Analysis. *Int. J. Numer. Methods Eng.* (1980) **15**:1862–1867.

[15] Aravas, N., On the numerical integration of a class of pressure-dependent plasticity models. *Int. J. Numer. Methods Eng.* (1987) **24**:1395–1416.

[16] Simo, J. C. and Taylor, R. L., Consistent tangent operators for rate-independent elastoplasticity. *Comput. Method Appl. M.* (1985) **48**:101–118.

[17] Prüger S. et al., A material model for TRIP-steels and its application to a CrMnNi cast alloy. *Steel Res. Int.* (2011) accepted for publication.